Geothermics 43 (2012) 57–65

Contents lists available at SciVerse ScienceDirect

Geothermics

journal homepage: www.elsevier.com/locate/geothermics

Optimization of energy extraction for closed shallow geothermal systems using linear programming

Michael de Paly[a,*], Jozsef Hecht-Méndez[b], Markus Beck[a], Philipp Blum[c], Andreas Zell[a], Peter Bayer[d]

[a] University of Tübingen, Wilhelm-Schickard-Institute for Computer Science (WSI), Sand 1, 72076 Tübingen, Germany
[b] University of Tübingen, Center for Applied Geoscience (ZAG), Sigwartstraße 10, 72076 Tübingen, Germany
[c] Karlsruhe Institute of Technology (KIT), Institute for Applied Geosciences (AGW), Kaiserstraße 12, 76131 Karlsruhe, Germany
[d] ETH Zürich, Engineering Geology, Sonneggstrasse 5, 8092 Zürich, Switzerland

ARTICLE INFO

Article history:
Received 21 January 2011
Accepted 19 March 2012
Available online 13 April 2012

Keywords:
Shallow geothermal systems
Sustainability
Optimization
Linear programming

ABSTRACT

The objective of the study is to optimize the performance and thereby to mitigate the environmental impact of ground source heat pump (GSHP) systems using multiple borehole heat exchangers (BHEs) by including variable energy loads. Hence, an optimization procedure is developed that is able to predict temperature distributions in the subsurface. Optimized BHE fields are able to keep the maximum temperature change in the subsurface about 18% lower than BHE fields which feature equal flow rates for all BHEs. The long-term temperature anomaly can be mitigated and the possibility of extracting a higher amount of energy, while keeping temperature thresholds or environmental constraints, arises.

1. Introduction

Shallow geothermal technologies that directly use the heat stored in the subsurface are counted among the most sustainable choices for space heating (Rybach and Mongillo, 2006; Saner et al., 2010). Depending on the supplied primary energy for the heat pumps and the efficiency of installation CO_2 can be avoided or even reduced (Nagano et al., 2006; Blum et al., 2010). In areas of normal or low geothermal gradient, heat pumps can be applied to extract the energy from depths down to about 400 m. Most often, closed or ground-coupled systems such as ground source heat pump (GSHP) systems are used (Lund et al., 2010). Depending on the heating demand, one or several vertical borehole exchangers (BHEs) are typically installed in the ground. The system is operated by circulating a heat carrier fluid in the BHEs, which exchanges heat with the ground and feeds an indoor heat pump. Even if shallow subsurface energy resources are enormous, local extraction causes temperature anomalies (Philippe et al., 2009; Hecht-Méndez et al., 2010). Natural heat conduction automatically balances these anomalies (Signorelli et al., 2004). However, replenishment needs time and hence the ground temperature should not be altered significantly. Ideally GSHP systems are run in seasonal mode, so that summer break is available for progressive replenishment of the energy deficit (Rybach and Eugster, 2010).

In order to ensure a lifetime of decades, it is crucial to configure the BHEs appropriately. This means that during the heating period the commonly rather low temperature of the ground should only be decreased by a few degrees. This condition is also necessary to maximize the performance of the heat pump, which is most efficient when the temperature increment between heat source and receiver is diminutive (e.g., Esen et al., 2008). In addition to technical issues environmental concerns might play a role such as the leakage of anti-freeze liquids used in BHEs (Klotzbücher et al., 2007; Saner et al., 2010) or the impact on the groundwater ecosystem by temperature changes (Brielmann et al., 2009, 2011). Sometimes artificial temperature changes are also regulated (Haehnlein et al., 2010). For example, in the state capital of Stuttgart in South Germany, the impact on the groundwater temperature in a distance of 50 m from a ground heat exchanger should be $\leq$2 K and for larger GSHP systems (>10 BHEs) a temperature monitoring is often required by the environmental authorities (Amt für Umweltschutz, 2005). Hence, it is desirable to mitigate the thermal impact of such systems on the subsurface and groundwater.

Appropriate configuration of single and multiple BHEs usually follows standardized recipes and apposite planning software such as Earth Energy Designer (EED), Transient System Simulation Program with the Duct Ground Storage model (TRNSYS-DST) and other programs are available (Schmidt and Hellström, 2005; Nagano et al., 2006). For technical or legal reasons, BHEs commonly are not implemented deeper than a few hundreds of meters (Haehnlein et al., 2010). If a single BHE is not sufficient to supply the energy required for a specific case, BHE fields are constructed, and the total BHE

* Corresponding author. Tel.: +49 7071 2978979; fax: +49 7071 295091.
E-mail address: michael@depaly.de (M. de Paly).

0375-6505/$ – see front matter © 2012 Elsevier Ltd. All rights reserved.
http://dx.doi.org/10.1016/j.geothermics.2012.03.001

length is oriented at the total energy demand. Depending on the specific case and available space, simple geometric arrangements such as square or longitudinal lattices are commonly selected (Fujii et al., 2005; Katsura et al., 2008, 2009). Usually, a distance of a few meters is considered sufficient to minimize mutual interference of adjacent BHEs, for example, from 3 m in China and up to 10 m in Germany (Kavanaugh and Rafferty, 1997; Signorelli et al., 2004; Haehnlein et al., 2010). BHE fields cause regional temperature anomalies, and projected to the surface these large scale temperature anomalies are composed of an array of tens to hundreds of concentric or elliptic temperature plumes that evolve around the BHEs. The larger the BHE field is the less effective the natural lateral conductive heat supply is, so that often the temperature within the field successively declines (Signorelli et al., 2004; Lazzari et al., 2010). Seasonal energy use in heating dominated operation is then reflected by periodic temperature variations that have a long-term decreasing trend (Diao et al., 2010). Accordingly, for a certain expected lifetime of a BHE field the final minimal ground temperature represents a crucial planning criterion. Thus, the aim is to keep the temperature decrease in the subsurface minimal while maximizing the technological performance of the BHEs.

In the present study, we identify thus far unconsidered degrees of freedom when planning BHE fields in conduction dominated media. In order to improve the concerted performance of multiple adjacent BHEs, the task is formulated as a mathematical optimization problem that is based on simulated superimposed BHE fields. Special attention is set on the heat transfer rates between the underground and the multiple BHEs that supply seasonal energy demands. Temperature changes in the underground exerted by multiple adjacent BHEs that operate with variable energy loads in heating mode are simulated. The temperature distribution can be predicted by numerical modeling (e.g., Bauer et al., 2011) or by spatial superposition of the infinite line source analytical solution (Carslaw and Jaeger, 1959). The time-dependent BHE-specific workloads are subdivided into step pulses and also superimposed (temporal superposition). An ideal energy extraction strategy is sought that takes into account the temperature changes in the underground and the time dependent heating demand. The optimal strategy supplies an effective input temperature to the heat pump and, therefore, is expected to improve the overall technical efficiency of the system compared to standard practice. Furthermore, the ideal solution should also guarantee lowest environmental impacts in the underground, i.e., aquifer temperatures should not be changed according to a pre-defined criterion or defined temperature limits and thresholds (Haehnlein et al., 2010).

Similar to previous work (e.g., Li et al., 2006, 2009; Katsura et al., 2008; Lazzari et al., 2010), we focus on optimization of BHE workloads (i.e., heat extraction rates). For example, Gao et al. (2010) present an operational strategy based on intermittent control of two BHEs; similarly, Cui et al. (2001) use discontinuous loads for the long-term operation of BHEs. While BHE specific loads can easily be simulated with the line source model, they do not exactly represent the real conditions in practice. In order to achieve a predefined load by an operating BHE, a control system that could, for example, adjust the flow rates of the heat carrier fluid would be necessary. Therefore, it is more common in practical applications to use equal flow rates for all BHEs, and by this, to indirectly obtain apposite BHE-specific energy extraction rates. Local low-temperature anomalies in the BHE field automatically lead to a smaller local energy extraction. Accordingly, in the well established BHE designing tools EED (Hellström and Sanner, 1997), and GLHEPRO (Spitler, 2000) the volumetric flow rate per borehole is uniformly distributed by the number of BHEs. A constant volumetric flow rate of the heat carrier can also be found in analytical and numerical simulation studies or performance investigations of multiple BHEs (Urchueguía et al., 2008; Katsura et al., 2009).

In the following, we will exploit the attractive properties from the analytical line source equation and, as a surrogate for flow rates, optimize BHE workloads in the field. The optimized solutions obtained by this proxy will be compared to standard practice, operating at equal flows and loads. The question is, even if flow regulation is not implicitly addressed in the mathematical formulation of the optimization problem, can the identified degrees of freedom be used to further improve BHE field design? To answer this question, the optimized results are compared to a BHE field implementation, in which a separate regulation of BHEs is not considered. Simulations by the Superposition Borehole Model (SBM, Eskilson, 1986; Pahud et al., 1996), which is able to compute underground and circulating fluid temperatures using the flow rates within the pipes, serve as a reference for the comparison.

2. Mathematical background

Symbol	Variable	Unit
COP	Coefficient of performance of the heat pump	–
E_l	Total energy demand for each time step	W
Ei	Exponential integral	–
EWT	Entering water temperature	K
i	Coordinate in the x-direction in field coordinates	m
j	Coordinate in the y-direction in field coordinates	m
L	Length of the BHE	m
q	Power demand/load	W
R_b	Thermal resistance of the borehole	m K W^{-1}
T	Temperature at the BHE location	K
T_b	Temperature at the borehole wall	K
T_u	Undisturbed temperature of the porous media	K
t	Time	s
x_k	Coordinate of BHE k in the x-direction	m
y_k	Coordinate of BHE k in the y-direction	m
z	Virtual variable	–
w	Weighting factor	–
λ	Thermal conductivity of the porous media	W m^{-1} K^{-1}
α	Thermal diffusivity	m^2 s^{-1}
ω	Response factor	–
k	Running index of BHEs	–
l	Running index of timesteps	–
m	Number of timesteps	–
n	Number of BHEs	–

2.1. Conductive heat transport in porous media (superposition principle)

A common approach for calculating two-dimensional (2D) radial temperature distribution in the underground due to the presence of a vertical BHE is the infinite line source model (Carslaw and Jaeger, 1959). Assuming an infinite homogeneous underground and a given energy transfer rate per unit length of the borehole, the temperature change ($\Delta T = T_u - T$) caused by a single BHE with load q and with T_u as the undisturbed temperature of the underground for a certain time (t) is expressed as:

$$\Delta T(\Delta x, \Delta y, t, q) = \frac{q}{4\pi L\lambda} Ei\left[\frac{(\Delta x^2 + \Delta y^2)^{0.5}}{4\alpha t}\right] \quad (1)$$

Ei is the so-called exponential integral, $\Delta x = (i - x_k)$ and $\Delta y = (j - y_k)$ are the distances to an arbitrary location (i,j) with respect to a BHE centered at (x_k,y_k), α is the thermal diffusivity and λ is the bulk thermal conductivity.

With the assumption that the soil thermal properties do not depend on temperature, i.e., Eq. (1) is linear with respect to q and, due to the fact that energy is an extensive and additive variable (Hellström, 1991; Yavuzturk et al., 1999; Diao et al., 2004;

Michopoulos and Kyriakis, 2009; Marcotte et al., 2010), the superposition principle can be applied to Eq. (1) as:

$$\Delta T_{i,j}(t, q_{k=1\ldots n}) = \sum_{k=1}^{n} \Delta T_k(i - x_k, j - y_k, t, q_k) \tag{2}$$

where n is the number of BHEs and T_k is the temperature change at (i,j) due to BHE k with an energy transfer rate q_k located at (x_k,y_k). When the workload q varies over time, it can be considered as a series of heating pulses (temporal superposition). This superposition of heat pulses has already been used in various previous works (Eskilson, 1987; Bernier et al., 2004; Marcotte and Pasquier, 2008; Michopoulos and Kyriakis, 2009; Marcotte et al., 2010). The variable energy extraction is subdivided into m time steps with constant load:

$$\Delta T(\Delta x, \Delta y, t, q_{l=1\ldots m}) = \sum_{l=1}^{m} \frac{q_l - q_{l-1}}{4\pi L\lambda} Ei\left[\frac{(\Delta x^2 + \Delta y^2)^{0.5}}{4\alpha(t_m - t_l)}\right] \tag{3}$$

where m is the total number of time steps and q_l is the load during time step l which runs from t_{l-1} to t_l, with $q_0 = 0$ and $t_0 = 0$.

By combining Eqs. (2) and (3), the temperature change at any arbitrary location in the subsurface exerted by multiple BHEs each with different time variable energy loads can be estimated through:

$$\Delta T_{i,j}(t, q_{1\ldots n,1\ldots m}) = \sum_{l=1}^{m}\sum_{k=1}^{n} q_{k,l}\omega_{k,l}^{t,i,j}(i - x_k, j - y_k) \tag{4}$$

With:

$$\omega_{k,l}^{t,i,j}(\Delta x, \Delta y) = \frac{1}{4\pi L\lambda}\left(Ei\left[\frac{(\Delta x^2 + \Delta y^2)^{0.5}}{4\alpha(t - t_{l-1})}\right] - Ei\left[\frac{(\Delta x^2 + \Delta y^2)^{0.5}}{4\alpha(t - t_l)}\right]\right) \tag{5}$$

as the response factor of BHE k on a position (i,j) within the BHE field at time step $l \in \{1,\ldots,m\}$ with reference to the current time step $t \in \{1,\ldots,m\}$ and $l \le t$ and $\Delta x = (i - x_k)$ and $\Delta y = (j - y_k)$.

By merging $q_{k,l}$ and $\omega_{k,l}^{t,i,j}$ into vectors of the form $\vec{q} = (q_{1,1}, \ldots, q_{n,1}, \ldots, q_{n,m})$ and $\vec{\omega}^{t,i,j} = (\omega_{1,1}^{t,i,j}, \ldots, \omega_{n,1}^{t,i,j}, \ldots, \omega_{n,m}^{t,i,j})$ Eq. (4) can be written as:

$$\Delta\vec{T}_{i,j}(t, \vec{q}) = \vec{q}(\vec{\omega}^{t,i,j})^T \tag{6}$$

where $\Delta\vec{T}_{i,j}(t, \vec{q})$ is the actual temperature change in the underground on the position (i,j) at time step t caused by the superposition of all BHEs in the field with the temporal load pattern $\vec{q}$.

2.2. Optimization objectives and constraints

The efficiency of the heat pump of a geothermal installation is mainly influenced by the fluid temperature coming from the BHE field which itself hugely depends on the temperature of the underground T. Therefore in the heating case, it is reasonable to keep $\min(T)$ as high as possible to keep the maximum observed cooling of the underground $\max(\Delta\vec{T}_{i,j})$ caused by the heat extraction through the BHEs as small as possible. As a result, extreme local cooling is avoided, the temperature distribution is smoothed, and potential ecological impacts from substantial local temperature gradients are mitigated. This leads to the primary objective of the proposed load assignment optimization:

$$\text{minimize}(\max(\Delta\vec{T}_{i,j})) \tag{7}$$

Depending on the field thermal parameters and the given load pattern the maximum overall temperature change may not be influenced by the load assignment for certain time steps. For these cases, which are otherwise not captured by the primary objective, we minimize the maximum temperature change within each time step as a secondary objective which is given a much lower weight than the primary objective.

In order to fulfill the energy demand required from the BHE field, the sum of the loads $q_{k,l}$ for each time step l has to equal to the required energy E_l for the given time step. This reads:

$$E_l = \sum_{k=1}^{n} q_{k,l} \quad l = 1\ldots m \tag{8}$$

2.3. Linear optimization procedure

Based on the definition of $\Delta\vec{T}_{i,j}(t, \vec{q})$ given in Eq. (6), the primary objective of minimization of the maximum overall temperature change for the entire considered time span given in Eq. (7) can be expressed as:

$$\arg\min(\max(\Delta\vec{T}_{i,j}(t, \vec{q}))) \quad \forall(i,j,t) \in S \tag{9}$$

where $\vec{q}$ is the decision variable and S is a set of all spatial and temporal reference points defined by 3-tuples (i,j,t).

In a similar manner the secondary objective of minimizing the temperature change within each single time step l can be written as:

$$\arg\min\left(\sum_{l=1}^{m}\max(\Delta\vec{T}_{i,j}(l, \vec{q}))\right) \quad \forall(i,j,t) \in S \quad t = l \tag{10}$$

In order to obtain a single objective function suitable for minimization, we combine the objective functions given in Eqs. (9) and (10) to:

$$\arg\min\left(w \cdot \max(\Delta\vec{T}_{i,j}(t, \vec{q})) + \sum_{l=1}^{m}\max(\Delta\vec{T}_{i,j}(l, \vec{q}))\right) \quad \forall(i,j,t) \in S \tag{11}$$

where w is a weighting factor which should be set to a large value to ensure the priority of the primary objective over the secondary objectives. w was set to 100 in this study.

Through the introduction of additional virtual variables $z_{0\ldots m}$ the max-norm terms of the objective function can then be rewritten as $m+1$ linear programs which minimize $z_{0\ldots m}$ and for every z reads:

$$\begin{aligned} &\min(z) \\ &\Delta\vec{T}_{i,j}(l, \vec{q}) - z\vec{e} \prec 0 \\ &-\Delta\vec{T}_{i,j}(l, \vec{q}) - z\vec{e} \prec 0 \end{aligned} \tag{12}$$

with $\vec{e}$ as the unity vector (Boyd and Vandenderghe, 2004).

Since the relationship between $\Delta\vec{T}$ and q is linear and between $\Delta\vec{T}_{i,j}$ and $\vec{q}$ is also linear, the energy load assignment problem can be posed as a linear program:

$$\min\left(w \cdot z_0 + \sum_{l=1}^{m} z_l\right) \tag{13}$$

subject to the constraints:

$$\begin{aligned} &\Delta\vec{T}_{i,j}(t, \vec{q}) - z_0 \prec 0 \\ &-\Delta\vec{T}_{i,j}(t, \vec{q}) - z_0 \prec 0 \end{aligned} \quad \forall(i,j,t) \in S$$

$$\begin{aligned} &\Delta\vec{T}_{i,j}(l, \vec{q}) - z_l \prec 0 \\ &-\Delta\vec{T}_{i,j}(l, \vec{q}) - z_l \prec 0 \end{aligned} \quad \forall(i,j,l) \in S \qquad l = 1\ldots m \tag{14}$$

where $z_{0\ldots m}$ and $\vec{q}$ are optimization variables.

The linear program is additionally constrained by the power demand for each time step which can be expressed as the equality constraint given in Eq. (8).

This is the monthly workload in case of a constant step size of 1 month between subsequent steps l. Since in our case we only

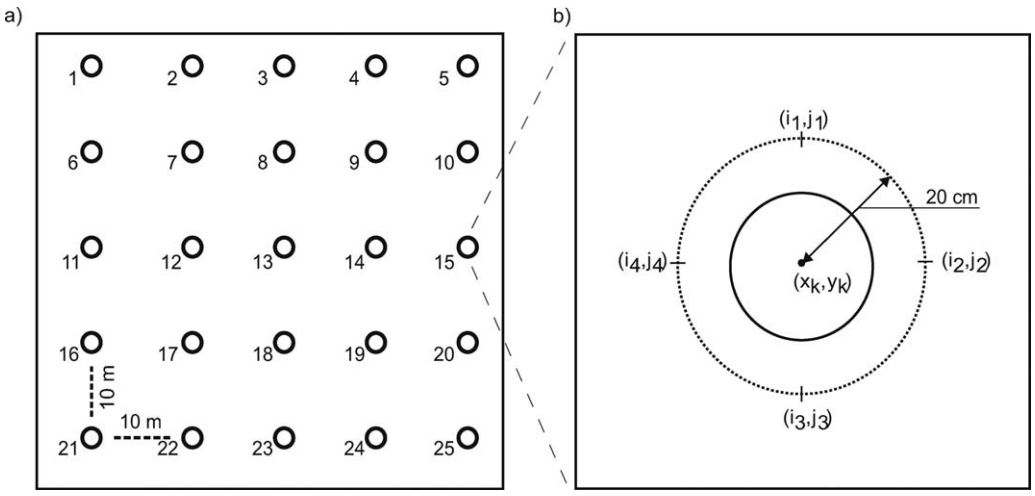

Fig. 1. (a) Top view of geothermal field with 25 BHEs used for applying the simulation-optimization procedure, (b) extended view of one BHE showing the reference points located around each BHE used for calculating a representative average borehole wall temperature.

consider heating, the load for each BHE for all time steps has to be positive. This results in the inequality constraint given by:

$$q_{k,l} \geq 0 \quad l = 1 \ldots m, \quad k = 1 \ldots n \tag{15}$$

Based on the formulation of the linear program given in Eqs. (11)–(15), the load assignment problem can be solved using standard linear program solvers such as CPLEX.

3. Model set up

In the present study a hypothetical BHE field scenario of 25 square lattice-like arranged BHEs with 10 m spacing ($\delta x = \delta y = 10$ m) and 100 m length each, which is similar to the study by Katsura et al. (2009), is considered as demonstration case for optimization of individual energy extractions (Fig. 1a). The subsurface geology is approximated as homogeneous and isotropic media. It is water-saturated and in this study no groundwater flow is considered, thus only conductive heat transport is addressed. Analytical simulation is performed for an operation period of 30 years with time variable BHE-specific energy loads. The geothermal system is optimized only for heating application, and no cooling is accounted for. As common for low-enthalpy geothermal simulations, temperature dependency of hydraulic (density and viscosity of the water) as well as of thermal parameters (thermal conductivity and volumetric heat capacity) is neglected (Hecht-Méndez et al., 2010).

As shown in Fig. 1b, four reference points for each BHE k are defined. These reference points are evenly distributed on a circle with a radius of 20 cm around the BHE position (x_k, y_k), which approximates the dimensions of the BHE. In order to estimate a single average subsurface temperature at the borehole wall for each BHE, we averaged $\Delta T_{i_{1\ldots4},j_{1\ldots4}}$ of the corresponding four reference points at each time step l. This results in n effective reference points in S for each time step l, respectively in $m \cdot n$ reference points for the whole optimization process. Thus for the considered time span (360 months) and the given BHE field (25 BHEs), the corresponding linear program consists of 9361 optimization variables, which can be subdivided into 361 virtual variables z and 9000 actual loads $q_{k,l}$. The number of constraints is 45,361. Assuming a subsurface composed of silts and clays, typical thermal parameters for groundwater saturated material are selected for the demonstration case (Table 1). The thermal parameters represent reference values for specific energy extraction of BHEs given by the German Engineer Association guideline for thermal use of the underground (VDI, 2001).

Table 1
Parameter specifications for demonstration case used for application of the simulation-optimization procedure.

Parameter	Unit	Value
Thermal conductivity (λ)[a]	$W\,m^{-1}\,K^{-1}$	1.70
Thermal diffusivity (α)[a]	$m^2\,s^{-1}$	7×10^{-7}
Length of the borehole (L)	m	100

[a] Values taken from VDI (2001).

Considering a heat transfer rate of 24 $W\,m^{-1}$ (VDI, 2001) and an annual runtime of 1800 h, the entire energy extraction of the BHE field is 108 MWh per year. The total energy extraction of 1 year is divided into 12 uneven intervals according to a monthly and individual heating demand typical for a GSHP system in Central Europe. Accordingly, an energy load profile for 1 year is defined, which is shown in Fig. 2. This profile approximates conditions applied in southern Germany by BHE-field designers, when no additional heat is required during the summer months. This profile is similar to the base load default profile of the EED software (version 3.15).

In the following sections, we will distinguish three cases: (i) the load optimized case, as described in the methodology section, (ii) the equal load case, which represents a non-optimized variant, assuming the same energy extraction for all BHEs, and (iii) the equal flow case, which corresponds to typical conditions of BHE fields in practice. The first two cases are simulated by the line source equation (Eq. (3)), whereas for the last case, equal volumetric flow rates of the circulating heat carrier fluid are obtained from the SBM model. The latter was applied to all (non-)optimized cases to

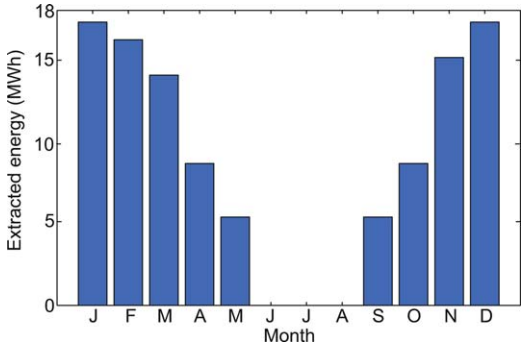

Fig. 2. Extracted energy per month of a GSHP system using 25 BHEs with a specific energy extraction of 24 $W\,m^{-1}$ and 1800 operating hours per year.

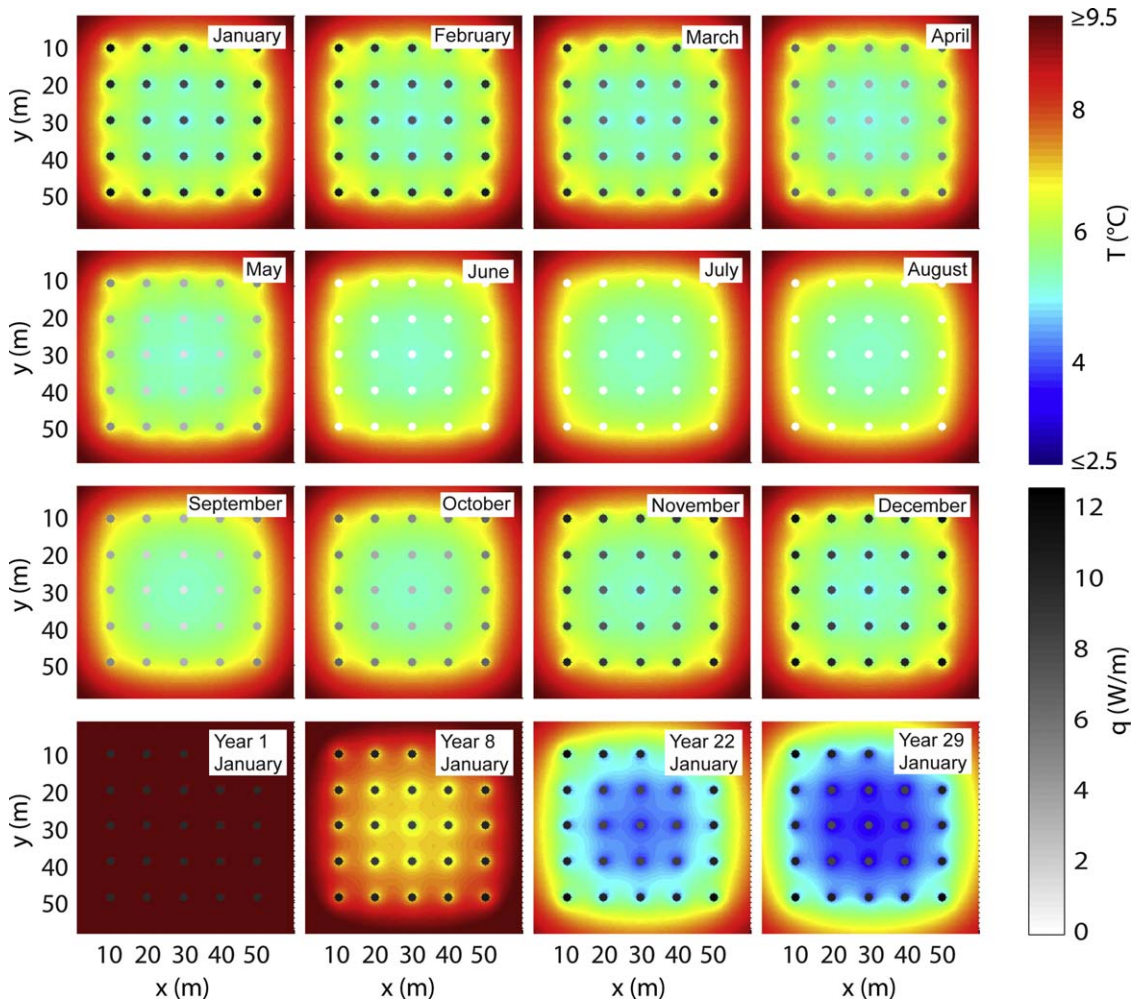

Fig. 3. Temperature distribution and BHE workloads for the non-optimized equal flow case. Each circle represents a BHE with its corresponding load in grayscale. Darker color shades denote higher BHE loads. The subsurface temperature distribution at a depth of 50 m is illustrated by colors, where high absolute temperatures appear in red and lower temperatures in blue. (For interpretation of the references to color in this figure legend, the reader is referred to the web version of the article.)

visualize the temperatures at 50 m depth and to compute the mixed outflow temperatures for all BHEs of the field, which enters the heat pump. SBM specific settings, which are used additionally to the values in Table 1, are listed in Table 2. These include fluid properties of water and assumed borehole resistances.

4. Results and discussion

Figs. 3–5 depict the BHE loads and the resulting temperature distribution in the subsurface for the non-optimized BHE fields with equal flow and equal loads and the load-optimized field, respectively. All three figures are divided into 16 subplots as follows: each subplot shows a combined load/temperature profile of the simulated BHE field for a defined time step t within 30 years of simulation time. The 12 subplots in the upper three rows visualize the month-wise development at half-time, that is, during the 15th operating year starting with January. The four lowermost subplots represent the temperature and load distributions for January of the 1st, 8th, 22nd and 29th years of operation and thus illustrate the long-term temperature trends of the installed BHE field. January is selected as the month with highest energy extraction and the largest temperature changes. BHEs are shown as gray shaded circles, where darker color shades denote higher BHE loads. Hence, switched-off BHEs are colored white and black BHEs are driven with the highest load possible during the actual time step. The subsurface temperature distribution (depth of 50 m) is illustrated by colors, where high absolute temperatures appear in red and lower temperatures in blue.

The three BHE field operation modes are simulated with the load profile depicted in Fig. 2. Thus, at each month all three fields extract the same amount of energy. For the optimized case (Fig. 5), the BHE loads are optimized individually for each BHE. In contrast, for the non-optimized cases (Figs. 3 and 4), the loads of all BHEs within the field are assigned the same loads, respectively the same heat carrier flow velocities.

As anticipated, optimized and equal loading of BHEs, as well as equal flow, result in symmetric temperature anomalies that develop in the ground. Further, as illustrated by the bottom plots in Figs. 3–5, the January records of the 1st, 8th, 22nd and 29th years reveal a continuous cooling of the BHE field. Apparently,

Table 2
Parameters specified in SBM.

Parameter	Unit	Value
Fluid viscosity (15 °C)	$kg\,m^{-1}\,s^{-1}$	1.14×10^{-3}
Fluid density	$kg\,m^{-3}$	1000
Fluid vol. heat capacity	$J\,m^{-3}\,K^{-1}$	4.1912×10^{6}
Fluid thermal conductivity	$W\,m^{-1}\,K^{-1}$	0.6
Borehole thermal resistance, R_b	$K\,W^{-1}\,m^{-1}$	0.0723
Borehole internal thermal resistance, R_a	$K\,W^{-1}\,m^{-1}$	0.2514

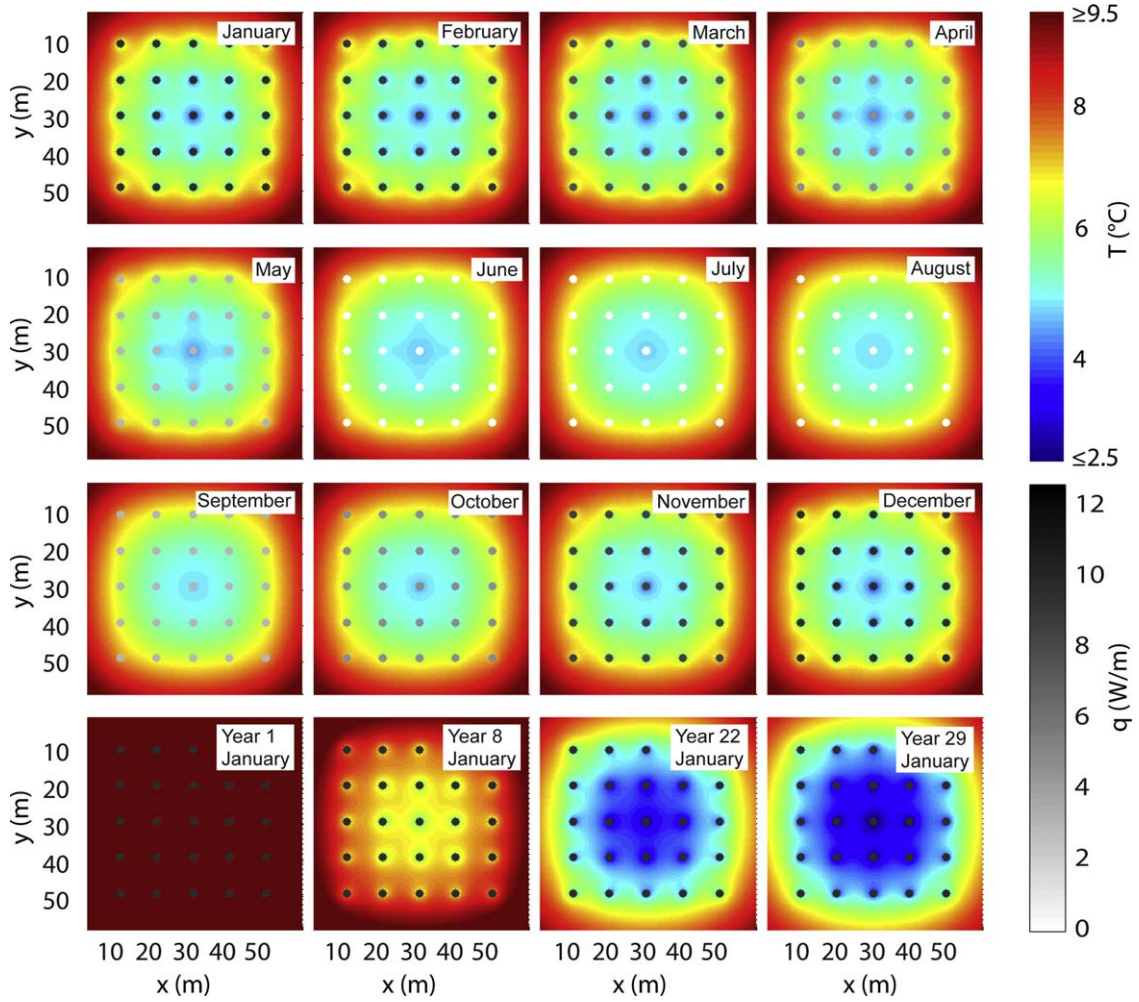

Fig. 4. Temperature distribution and BHE workloads for the non-optimized equal load case. Each circle represents a BHE with its corresponding load in grayscale. Darker color shades denote higher BHE loads. The subsurface temperature distribution at a depth of 50 m is illustrated by colors, where high absolute temperatures appear in red and lower temperatures in blue. Please note: for a given month all BHE have equal load. The impression of slightly varying shades of gray is an optical illusion caused by differing background coloring. (For interpretation of the references to color in this figure legend, the reader is referred to the web version of the article.)

the regeneration time during the summer period is too short to balance the deficit by conductive lateral heat supply in all three cases, which is a well-known long-term behavior of such GSHP systems (Eugster and Rybach, 2000). This is also reflected by the small changes that can be observed during the small or no energy extraction phase in the summer season between May and August.

Figs. 3–5 reveal that long-term BHE operations can generate substantially decreased temperatures that locally fall below 2.5 °C. The relatively high observed temperature changes, ΔT, correspond to the results of recent investigations, for instance by Priarone et al. (2009), who obtained even higher values for heating dominated cases with large BHE fields. Rybach and Eugster (2010) observed similar values close to the borehole wall of a single BHE application at the Elgg site in Switzerland. Since the relationship between ΔT and the loads $\bar{q}$ is linear, ΔT can easily be limited to a desired value of ΔT by scaling the $\bar{q}$ obtained from the optimizer with the ratio between the desired ΔT and the actual ΔT. In other words, the relative difference between optimized and non-optimized BHE fields remains the same even if much smaller total specific heat extraction rates are assumed and/or a stricter ΔT constraint has to be obeyed.

At first sight, the differences between the three cases do not appear significant. While equal flows and workloads tend to generate local anomalies in the BHE field, the optimized system yields more smoothed temperature contours. The temperature anomalies successively develop for all operation modes, but are most concentrated in the equal load case. This reflects that, in particular, the interior BHEs in the field are insulated by the outer BHEs, which averts sufficient conductive energy supply from the ambient ground. Even in the equal flow case, which represents a self-regulated system, where heat transfer is automatically smaller in low-temperature regions, a similar trend can be observed. Central BHEs cool the ground much more than the outer BHEs. Still, this case, which represents standard practice, performs better than the more hypothetical equal load case: the low temperature extremes are less pronounced after the full operation period of 30 years (Figs. 3–5).

Figs. 3 and 5 show that the load distribution does not exhibit equal extraction rates for all BHEs during equal flow and optimized load operation modes. In fact, the individual BHE loads crucially differ depending on the position of the individual BHE within the field and at a certain time-step. While for equal flow this is self-regulated according to the temperature gradients at each BHE, load optimization yields a system-specific strategy. It turns out that it is beneficial to deactivate the BHEs with the largest influence on neighboring BHEs, starting at the months with lowest energy demand, and to reactivate them when the energy demand rises again. Thus, the global optimum for the used load profile suggests deactivating first

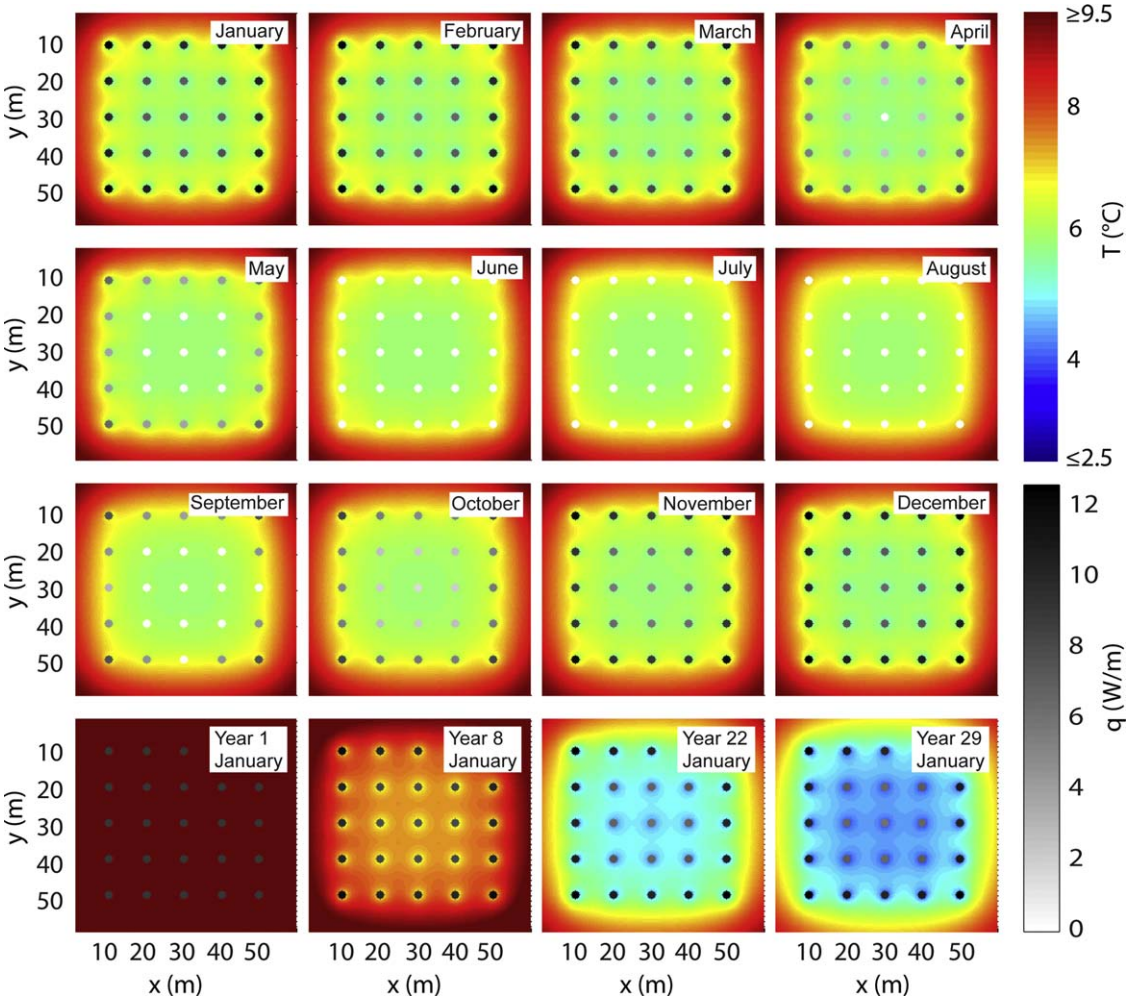

Fig. 5. Temperature distribution and BHE workloads for the optimized case. Each circle represents a BHE with its corresponding load in grayscale. Darker color shades denote higher BHE loads. The subsurface temperature distribution at a depth of 50 m is illustrated by colors, where high absolute temperatures appear in red and lower temperatures in blue. (For interpretation of the references to color in this figure legend, the reader is referred to the web version of the article.)

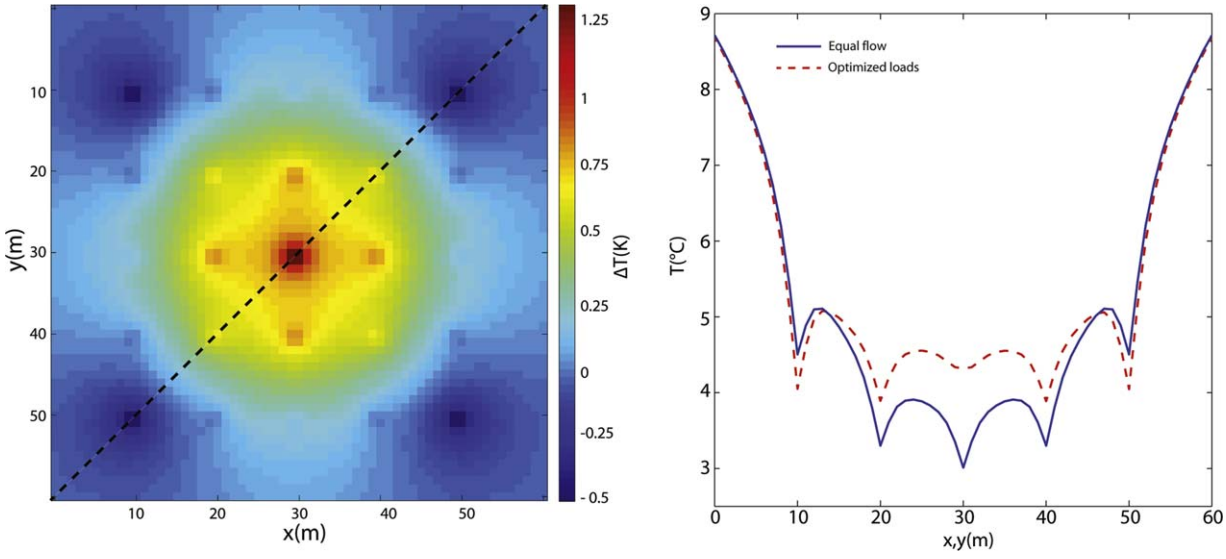

Fig. 6. Temperature differences in the subsurface between the optimized and the equal flow case at the end of the heating period (March) of the final year (30) of the simulated time frame. (a) Shows the areal temperature difference at 50 m depth between both cases. (b) Depicts a cross section of the temperature change from one corner of the BHE field to the opposed one (dashed line in a).

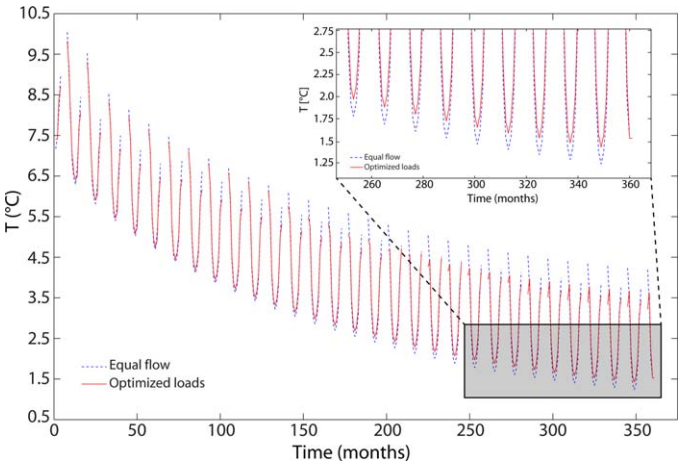

Fig. 7. Mixed temperature evolution of the working fluid of all BHEs in the field. The mixed outflow temperature is depicted in blue for the equal flow case and in red for the optimized case. The zoomed section highlights the permanently higher temperatures of the optimized case. (For interpretation of the references to color in this figure legend, the reader is referred to the web version of the article.)

the BHEs in the center of the field in April of each year (BHEs: 8, 12, 13, 14 and 18). In September, when energy extraction starts again after the summer months, first the BHEs at the outer edge of the field (BHEs: 1–6, 10, 11, 15, 16, 20–25) should be reactivated. As a result, local temperature anomalies are mitigated, and a more balanced lateral cooling of the ground is achieved. This is illustrated in more detail in Fig. 6, which inspects the underground temperature after the heating period in the final year. Fig. 6a shows the areal temperature difference in 50 m depth between both cases. Additionally, a cross section of the temperature change along the dashed line is depicted in Fig. 6b. The differences in Fig. 6a reach up to 1.25 °C (i.e., 18%), which represents the strongest cooling at the central BHE. By load optimization, the lower central heat extraction is compensated by relatively higher loads at the BHE field boundary. This is reflected by the areas (dark blue) at the fringe with negative temperature differences, and shown in Fig. 6b when comparing the temperatures of the BHEs at a distance of 10 m and then 50 m from the corner of the field. Another aspect that can be extracted from the plots in Fig. 6 is that even if the optimized system does not manage to generate equal temperatures, the variability is much less pronounced. The positive differences in the center of the field demarcate relative higher cooling by the equal flow case when compared to the optimized case. These are considerably more severe than the negative differences which are located at the fringe of the field.

Of special interest is the temperature that arrives at the heat pump, which can also be used to compare the three different operation modes. The lower this temperature is, the smaller the expected seasonal performance factor and thus the worse the efficiency of the entire geothermal heating system. Fig. 7 reports the mixed outflow temperature evolution of the working fluid of all BHEs of the non optimized equal flow case and the load optimized case in the field. These are obtained by averaging the monthly BHE-specific outflow temperatures simulated by SBM. Similar to the findings from previous studies (e.g., Signorelli et al., 2004), sinusoidal oscillation reflects alternating use phases and regeneration phases. Since the subsurface is not able to regenerate during the course of the year, annual mean temperatures decline with progressing use. Due to averaging, the differences between the two cases are only very small. Obviously, mixing rules out the extremes as observed when comparing the in situ temperature distribution (Figs. 3–6). Even so, as highlighted in the zoomed section in Fig. 7, the optimized load case yields slightly higher temperatures than the alternative cases. This demonstrates that even if loads are used as proxy for the combined simulation-optimization, better strategies can be found than standard practice. Since the difference is rather small, however, in practice slight performance improvement potential may not be sufficient for justifying the application of additional control systems. In fact, the advantage of an optimized system is the possibility to extract a higher amount of energy while complying with given temperature thresholds or environmental constraints.

5. Conclusions

A new approach for the optimization of scheduled energy extraction of closed shallow geothermal systems based on linear programming is presented. In this work, flow regulation is not implicitly addressed in the mathematical formulation of the optimization problem, thus BHE workloads will be optimized as a surrogate for flow rates. Combined spatial and temporal superposition of the infinite line source analytical solution is used to simulate temperature changes in the underground caused by multiple adjacent borehole heat exchangers (BHEs), which operate with variable energy loads. By exploiting the linear relationship between the individual loads of the BHEs and the temperature changes in the underground we are able to formulate a linear optimization problem for assigning globally optimal loads for each BHE for each time step. The optimization objective is to minimize the ground temperature changes and therefore maximize heat pump performance, comply with regulative thresholds for induced temperature changes and mitigate environmental impacts. To determine if the workload optimization allows for improvement of BHE field design even without considering flow regulation, the optimized solutions obtained by this proxy were compared to a BHE field implementation, which operates at equal flows and loads. Except for the optimization step, all simulations were accomplished by the SBM code (Eskilson, 1986; Pahud et al., 1996).

The procedure is demonstrated for a simplified hypothetical case with 25 BHEs that are operated for 30 years to accomplish seasonally variable heating energy requirements typical for larger office buildings, schools or district heating systems. In the current study only heat conduction, i.e., no significant groundwater flow is considered in a homogeneous ground. The optimized BHE fields result in a mitigation of long-term temperature decrease and local temperature anomalies, and a more balanced, more lateral cooling of the ground is achieved. Current practical applications using equal flow rates for all BHEs achieve acceptable mixed outflow temperatures, but the absolute temperature decrease in the subsurface can additionally be diminished up to 18% if optimization is incorporated. This instance allows for significantly higher energy extraction rates without increasing environmental impacts and respectively a better compliance with statutory provisions. Since the developed optimization method does not distinguish between any assumptions regarding the geometry of the field and the geological, hydrogeological and thermal parameters of the ground, it can be easily transferred to other cases and be readily implemented in planning software. Depending on the specific problem, the selected monthly resolution of the load profile can also be replaced by a coarser or finer resolution. As an extension, cooling can be accounted for. Almost any given BHE field geometry can be inspected, if the underlying superposition assumptions hold. However, since the mutual impact factors of the BHEs in the field are calculated using the infinite line source model, the presented method can currently only be used for conductive cases without groundwater flow. Alternative BHE simulation would therefore be necessary, if advective heat transport in the ground is significant. Likewise, the optimization procedure can also be extended for additional analytical solutions, as for instance the finite line

source model (Zeng et al., 2002) or finite moving line source model (Molina-Giraldo et al., 2011).

Large matrices are utilized to represent the mutual influence coefficients between the BHEs for all time steps. Implemented in a computer, they easily grow to several gigabytes in size. This sets an upper limit on the number of BHEs and of time steps depending on the platform used. The computational time was approximately 30 min for the calculation of the coefficients ω and 3 h for solving the linear program on a 3.6 GHz quadcore CPU utilizing 6 GB of RAM. In view of the growing computational power, however this is not considered to be a severe shortcoming in the future. As a remedy, it is often desirable to search for close-optimal solutions that can be obtained by separation of the full operation problem into sub-problems, e.g., by successively optimized separate operation intervals.

Acknowledgements

This work was supported by the Deutsche Bundesstiftung Umwelt (DBU), the EU FP7 ECO-GHP project, and the Federal Ministry for Education and Research (BMBF) scholarship program for International Postgraduate Studies in Water Technologies (IPSWaT). We thank David Kuntz for providing the load profile used in this study. We would also like to thank Daniel Pahud for providing the SBM model and the reviewers who helped to considerably improve the paper with their constructive feedback.

References

Amt für Umweltschutz Landeshauptstadt Stuttgart, 2005. Nutzung der Geothermie in Stuttgart. Schriftreihe des Amtes für Umweltschutz, Heft 1/2005, 89 pp.

Bauer, D., Heidemanna, W., Diersch, H.-J.G., 2011. Transient 3D analysis of borehole heat exchanger modeling. Geothermics 40 (4), 250–260.

Bernier, M.A., Pinel, P., Labib, R., Paillot, R., 2004. A multiple load aggregation algorithm for annual hourly simulations of GCHP systems. HVAC & R Research Journal 10 (4), 471–488.

Blum, P., Campillo, G., Münch, W., Kölbel, T., 2010. CO_2 savings of ground source heat pump systems – a regional analysis. Renewable Energy 35, 122–127.

Boyd, S., Vandenderghe, L., 2004. Convex Optimization. Cambridge University Press, Cambridge, 697 pp.

Brielmann, H., Griebler, C., Schmidt, S.I., Michel, R., Lueders, T., 2009. Effects of thermal energy discharge on shallow groundwater ecosystems. FEMS Microbiology Ecology 68 (3), 273–286.

Brielmann, H., Lueders, T., Schreglmann, K., Ferraro, F., Blum, P., Bayer, P., Hammerl, V., Griebler, C., 2011. Oberflächennahe Geothermie und ihre potentiellen Auswirkungen auf die Grundwasserökologie. Grundwasser 16 (2), 77–91.

Carslaw, H.S., Jaeger, J.C., 1959. Conduction of Heat in Solids. Oxford University Press, New York, NY, USA, 510 pp.

Cui, P., Diao, N.R., Fang, Z.H., 2001. Analysis on discontinuous operation of geothermal heat exchangers of the ground-source heat pump systems. Journal of Shandong Institute of Architecture and Engineering 16, 52–57.

Diao, N., Cui, P., Liu, J., Fang, Z., 2010. R&D of the ground-coupled heat pump technology in China. Frontiers of Energy and Power Engineering in China 4, 47–54.

Diao, N., Li, Q., Fang, Z., 2004. Heat transfer in ground heat exchangers with groundwater advection. International Journal of Thermal Sciences 43, 1203–1211.

Esen, H., Inalli, M., Sengur, A., Esen, M., 2008. Predicting performance of a ground-source heat pump system using fuzzy weighted pre-processing-based ANFIS. Building and Environment 43 (12), 2178–2187.

Eskilson, P., 1986. Superposition Borehole Model. Manual for Computer Code. Department of Mathematical Physics, University of Lund, Lund, Sweden, 144 pp.

Eskilson, P., 1987. Thermal Analysis of Heat Extraction Boreholes. Department of Mathematical Physics, University of Lund, Lund, 222 pp.

Eugster, W.J., Rybach, L., 2000. Sustainable production from borehole heat exchanger systems. In: Proceedings World Geothermal Congress, Kyushu-Tohoku, Japan, pp. 825–830.

Fujii, H., Itoi, R., Fujii, J., Uchida, Y., 2005. Optimizing the design of large-scale ground-coupled heat pump systems using groundwater and heat transport modeling. Geothermics 34, 347–364.

Gao, Q., Li, M., Yu, M., 2010. Experiment and simulation of temperature characteristics of intermittently-controlled ground heat exchanges. Renewable Energy 35, 1169–1174.

Haehnlein, S., Bayer, P., Blum, P., 2010. International legal status of the use of shallow geothermal energy. Renewable and Sustainable Energy Reviews 14, 2611–2625.

Hecht-Méndez, J., Molina-Giraldo, N., Blum, P., Bayer, P., 2010. Evaluating MT3DMS for heat transport simulation of closed geothermal systems. Ground Water 48, 741–756.

Hellström, G., 1991. Ground Heat Storage: Thermal Analysis of Duct Storage Systems. I. Theory. Department of Mathematical Physics, University of Lund, Lund, 262 pp.

Hellström, G., Sanner, B., 1997. EED – Earth Energy Designer, Version 1.0, User's Manual. Wetzlar, Germany, 43 pp.

Katsura, T., Nagano, K., Narita, S., Takeda, S., Nakamura, Y., Okamoto, A., 2009. Calculation algorithm of the temperatures for pipe arrangement of multiple ground heat exchangers. Applied Thermal Engineering 29, 906–919.

Katsura, T., Nagano, K., Takeda, S., 2008. Method of calculation of the ground temperature for multiple ground heat exchangers. Applied Thermal Engineering 28, 1995–2004.

Kavanaugh, S.P., Rafferty, K.D., 1997. Ground Source Heat Pumps: Design of Geothermal Systems for Commercial and Institutional Buildings. ASHRAE, Atlanta, 167 pp.

Klotzbücher, T., Kappler, A., Straub, K.L., Haderlein, S.B., 2007. Biodegradability and groundwater pollutant potential of organic anti-freeze liquids used in borehole heat exchangers. Geothermics 36, 348–361.

Lazzari, S., Priarone, A., Zanchini, E., 2010. Long-term performance of BHE (borehole heat exchanger) fields with negligible groundwater movement. Energy 35, 4966–4974.

Li, S., Yang, W., Zhang, X., 2009. Soil temperature distribution around a U-tube heat exchanger in a multi-function ground source heat pump system. Applied Thermal Engineering 29, 3679–3686.

Li, X., Chen, Z., Zhao, J., 2006. Simulation and experiment on the thermal performance of U-vertical ground coupled heat exchanger. Applied Thermal Engineering 26, 1564–1571.

Lund, J.W., Freeston, D.H., Boyd, T.L., 2010. Direct utilization of geothermal energy 2010 worldwide review. In: Proceedings 2010 World Geothermal Congress, Bali, Indonesia, 25–29 April, 23 pp.

Marcotte, D., Pasquier, P., 2008. Fast fluid and ground temperature computation for geothermal ground-loop heat exchanger systems. Geothermics 37 (6), 651–665.

Marcotte, D., Pasquier, P., Sheriff, F., Bernier, M., 2010. The importance of axial effects for borehole design of geothermal heat-pump systems. Renewable Energy 35 (4), 763–770.

Michopoulos, A., Kyriakis, N., 2009. A new energy analysis tool for ground source heat pump systems. Energy and Buildings 41, 937–941.

Molina-Giraldo, N., Blum, P., Zhu, K., Bayer, P., Fang, Z., 2011. A finite line source model to simulate borehole heat exchangers with groundwater advection. International Journal of Thermal Sciences 50 (12), 2506–2513, http://dx.doi.org/10.1016/j.ijthermalsci.2011.06.012.

Nagano, K., Katsura, T., Takeda, S., 2006. Development of a design and performance prediction tool for the ground source heat pump system. Applied Thermal Engineering 26, 1578–1592.

Pahud, D., Fromentin, A., Hadorn, J.C., 1996. The Superposition Borehole Model for TRNSYS (TRNSBM). User Manual for the November 1996 Version. Internal Report. LASEN-DGC-EPFL, Switzerland, 95 pp.

Philippe, M., Bernier, M., Marchio, D., 2009. Validity ranges of three analytical solutions to heat transfer in the vicinity of single boreholes. Geothermics 38, 407–413.

Priarone, A., Lazzari, S., Zanchini, E., 2009. Numerical evaluation of long-term performance of borehole heat exchanger fields. In: Proceedings of the COMSOL Conference, Milano, 6 pp.

Rybach, L., Eugster, W.J., 2010. Sustainability aspects of geothermal heat pump operation, with experience from Switzerland. Geothermics 39, 365–369.

Rybach, L., Mongillo, M., 2006. Geothermal sustainability – a review with identified research needs. Geothermal Resource Council Transactions 30, 1083–1090.

Saner, D., Juraske, R., Kübert, M., Blum, P., Hellweg, S., Bayer, P., 2010. Is it only CO_2 that matters? A life cycle perspective on shallow geothermal systems. Renewable and Sustainable Energy Reviews 14, 1798–1813.

Schmidt, T., Hellström, G., 2005. Ground Source Cooling – Working Paper on Usable Tools and Methods. EU Commission SAVE Program and Nordic Energy Research, 21 pp.

Signorelli, S., Kohl, T., Rybach, L., 2004. Sustainability of production from borehole heat exchanger fields. In: Proceeding Twenty-Ninth Workshop on Geothermal Reservoir Engineering, Stanford, January 26–28, 2004, 6 pp.

Spitler, J.D., 2000. GLHEPRO – a design tool for commercial building ground loop heat exchangers. In: Proceedings of the Fourth International Conference of Heat Pumps in Cold Climates, Aylmer, Québec, 17–18 August 2000, pp. 1–15.

Urchueguía, J.F., Zacarés, M., Corberán, J.M., Montero, Á., Martos, J., Witte, H., 2008. Comparison between the energy performance of a ground coupled water to water heat pump system and an air to water heat pump system for heating and cooling in typical conditions of the European Mediterranean coast. Energy Conversion and Management 49, 2917–2923.

VDI, 2001. Thermal Use of the Underground. Part 2: Geothermal Heat Pump Systems. VDI-Verlag, VDI 4640, Düsseldorf, 43 pp.

Yavuzturk, C., Spitler, J.D., Rees, S.J., 1999. A transient two-dimensional finite volume model for the simulation of vertical U-tube ground heat exchangers. ASHRAE Transactions 105 (2), 465–474.

Zeng, H.Y., Diao, N.R., Fang, Z.H., 2002. A finite line-source model for boreholes in geothermal heat exchangers. Heat Transfer-Asian Research 31, 558–567.